Supporting Information

Facile synthesis of ultrathin ZIF-67 layer on the surface of Sn/Ti co-doped hematite for efficient photoelectrochemical water oxidation

Pan Huang,[a] Xuan Miao,[b] Juan Wu,[c] Peng Zhang,[a] Hongbi Zhang,[a] Shiqiang Bai[a] and Weisheng Liu*[a]

[a]*The Key Laboratory of Nonferrous Metal Chemistry and Resources Utilization of Gansu Province, State Key Laboratory of Applied Organic Chemistry, College of Chemistry and Chemical Engineering, Lanzhou University, Lanzhou, 730000, P.R. China. E-mail: liuws@lzu.edu.cn*

[b]*School of Physical Science and Technology, Lanzhou University, Lanzhou, 730000, P.R. China.*

[c]*The Key Laboratory of Rare Earth Functional Materials and Applications, International Joint Research Laboratory for Biomedical Nanomaterials of Henan, Zhoukou Normal University, Zhoukou, 466001, P.R. China.*

*Corresponding author: liuws@lzu.edu.cn

Materials and Reagents

All reagents and solvents employed were commercially available and used as received without further purification. Iron chloride hexahydrate, Cobalt nitrate hexahydrate and 2-Methylimidazole were purchased from Aladdin Industrial Corporation (Shanghai, China). Urea, Potassium hydroxide and Tin (II) chloride dihydrate were purchased from Chron Chemicals Co.,Ltd (Chengdu, China). Titanium tetrachloride was purchased from Beijing Innochem Science & Technology Co.,Ltd (Beijing, China). Sodium sulfite was purchased from Sinopharm Chemical Reagent Co., Ltd (Shanghai, China).

Fluorine-doped tin oxide-coated glass (FTO, < 10 Ω/sq, 1 cm × 4 cm × 2.2 mm) was purchased from Foshan Yuanjingmei Glass Co., Ltd (Foshan, China). Deionized water (18.2 MΩ cm) was used in all experiments.

Characterizations

The XRD spectra were measured to record the crystal structures on a Rigaku D/max 2400 instrument. The morphological feature was analyzed by FESEM (Apreo S) and HRTEM (Philips Tecnai F30). X-ray photoelectron spectroscopy analysis was performed using XPS spectrometers (Kratos AXIS Ultra DLD). The optical absorption of the photoanodes was determined by an UV−vis−NIR spectrophotometer (Cary 5000). The PL was measured using fluorescence spectroscopy (Hitachi F-7000) with light at an excitation wavelength of 415 nm at ambient temperature. Inductively coupled plasma optical emission spectrometry (ICP-OES) was obtained on a Plasma Quant PQ9000.

Photoelectrochemical (PEC) measurements

The PEC measurements of all photoanodes were achieved on the CHI660B electrochemical workstation (CH Instruments Co.) in a standard three-electrode system containing the photoanodes (WE), a Pt fossil (1 × 1 cm^2, CE), a saturated Ag/AgCl electrode (RE). The electrolyte was a 1 mol L^{-1} potassium hydroxide solution (pH = 13.6). To simulate AM 1.5G sunlight, a 300 W Xe lamp was used. The LSV curves were plotted using a potential of 0.5−1.5 V *vs.* RHE. The EIS Nyquist plots were collected at a bias of 0.05 V (*vs.* Ag/AgCl) with a frequency range of 0.01−100,000 Hz under AM 1.5 G (100 mW cm^{-2}) illumination.

Equations in this work

1. Mott-Schottky measurement

M-S plots were collected at an AC frequency of 1 kHz in the dark, and the N_D of the photoanodes could be estimated by the following equation:

$$N_D=\frac{2}{e\varepsilon\varepsilon_0\left[\frac{d\left(\frac{1}{C^2}\right)}{dV}\right]^{-1}} \quad \textbf{equation S1}$$

Where, C is the space charge capacitance in the semiconductor (obtained from M-S curves), e is the electron charge, ε is the vacuum permittivity (8.85×10^{-12} F m^{-1}), ε_0 is the relative dielectric constant of hematite ($\varepsilon_0 = 80$), N_D is the charge donor density (cm^{-3}), V is the electrode applied potential.

2. Light harvesting efficiency (LHE)

LHE is defined as the fraction of photons absorbed per photons impinging on the sample, which could be calculated using the following equation:

$$LHE=1-10^{-A(\lambda)} \quad \textbf{equation S2}$$

A(λ) is the absorbance at a specific wavelength.

3. Theoretical maximum photocurrent density (J_{abs})

Theoretical maximum photocurrent density (J_{abs}) is the photocurrent density assuming that all absorbed photons can be converted into current, it is a constant with the AM 1.5 G spectrum and the light harvesting efficiency of the fixed photoelectrode. In the case of J_{abs}, it can be calculated according to the following equation:

$$J_{abs}=\int_{\lambda_1}^{\lambda_2}\frac{\lambda\times LHE(\lambda)\times P(\lambda)}{1240}d(\lambda) \quad \textbf{equation S3}$$

where λ and P(λ) are the light wavelength (nm) and the corresponding power density (mW cm^{-2} nm^{-1}) for the standard solar spectrum AM 1.5G (ASTMG-173-03), respectively.

4. The surface charge injection efficiency ($\eta_{surface}$) and bulk charge separation efficiency (η_{bulk})

Photocurrent density arising from PEC water oxidation can be described by the following equation：

$$J_{H_2O} = J_{abs} \times \eta_{bulk} \times \eta_{surface}$$ **equation S4**

η_{bulk} is the yield of photo-induced holes which have migrated to the semiconductor-electrolyte interfaces and $\eta_{surface}$ is the yield of holes which are involved in water oxidation reaction. In this work, we chose the widely used Na_2SO_3 as the hole scavenger. Moreover, η_{bulk} and $\eta_{surface}$ were calculated according to the equations, respectively：

$$\eta_{bulk} = \frac{J_{Na_2SO_3}}{J_{abs}}$$ **equation S5**

$$\eta_{surface} = \frac{J_{H2O}}{J_{Na_2SO_3}}$$ **equation S6**

$J_{Na_2SO_3}$ and J_{H2O} are the photocurrent densities measured in 1 M KOH with and without 1 M Na_2SO_3, respectively

5. Calculation of the Applied bias photo-to-current conversion efficiency (ABPE)

Assuming 100% Faradaic efficiency, the ABPE was obtained by the following equation:

$$ABPE(\%) = J \times \frac{1.23 - E_{RHE}}{P} \times 100\%$$ **equation S7**

Where *J* represents the photocurrent density (mA·cm^{-2}) at the applied bias V *vs.* RHE, E_{RHE} is the applied bias at the reversible hydrogen electrode (RHE) condition, *P* is the incident light intensity (mW·cm^{-2}).

6. Calculation of the Incident photo-to-electron conversion efficiency (IPCE):

$$IPCE(\%) = (1240 \times J)/(\lambda \times P)$$ **equation S8**

Where J is the photocurrent density (mA·cm^{-2}) at the applied bias V vs. RHE, λ is the wavelength of incident light (nm), P is the incident light intensity(mW·cm^{-2}).

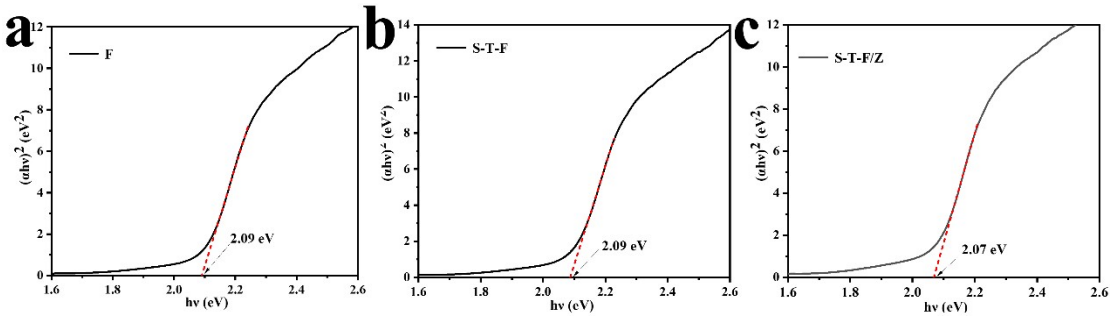

Fig. S1 (a), (b) and (c) Fitted band-gaps of F, S-T-F and S-T-F/Z photoanode, respectively.

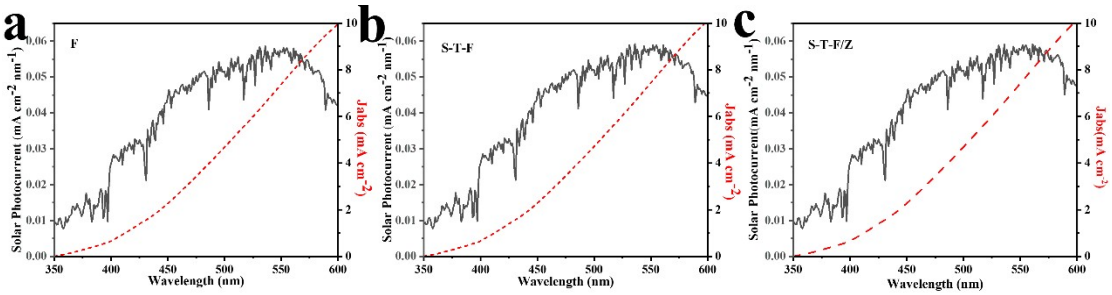

Fig. S2 (a), (b) and (c) J_{abs} (assuming 100% absorbed photo-to-current conversion efficiency for photons) of F, S-T-F and S-T-F/Z photoanode, respectively.

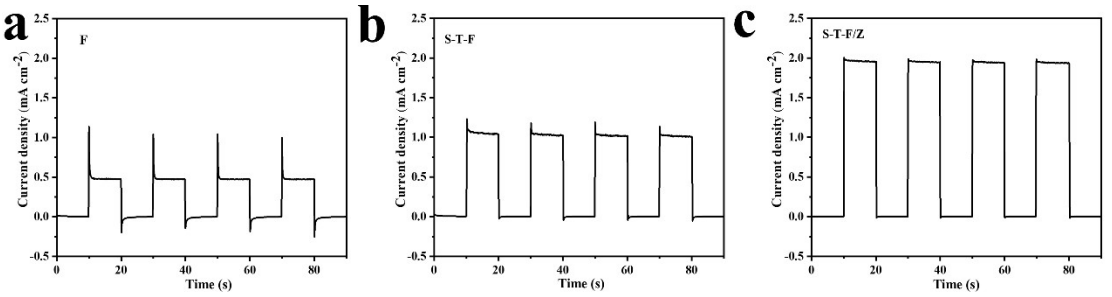

Fig. S3 (a), (b) and (c) Chronoamperometric I−t curves at 1.23 V *vs*. RHE of F, S-T-F and S-T-F/Z photoanode, respectively.

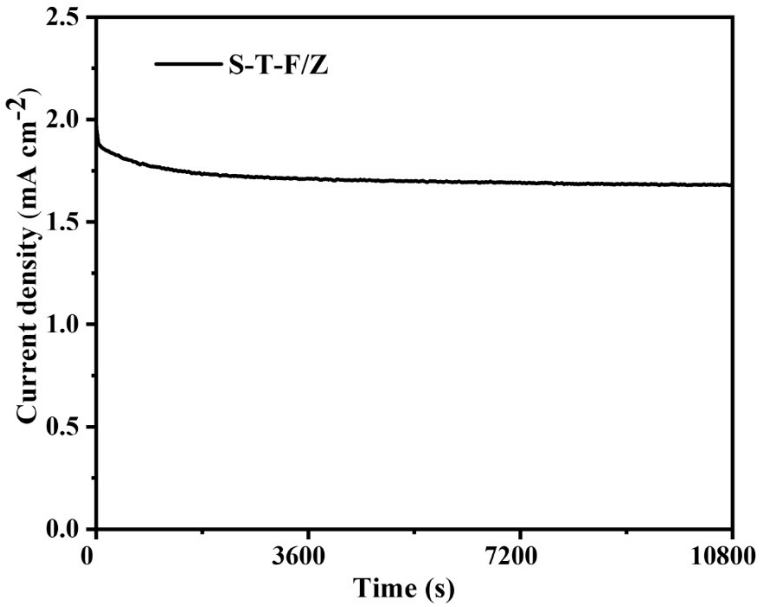

Fig. S4 Chronoamperometry curve of S-T-F/Z photoanode at 1.23 V *vs*. RHE.

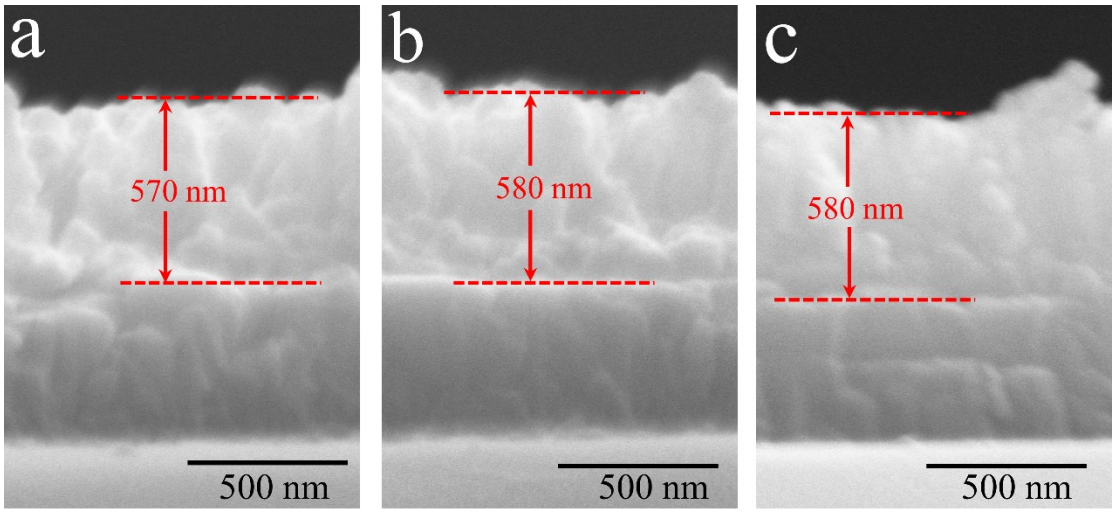

Fig. S5 (a), (b) and (c) cross-sectional SEM image of F, S-T-F and S-T-F/Z photoanode, respectively.

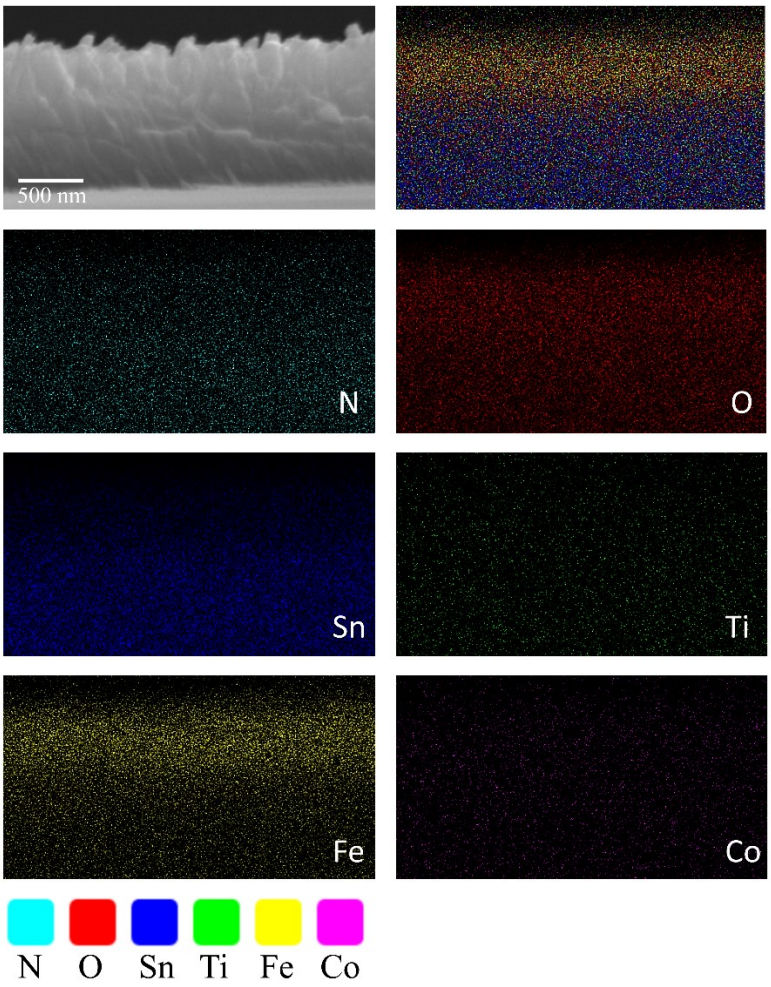

Fig. S6 SEM-EDX element mapping for Fe, O, Ti, Sn, Co and N of S-T-F/Z photoanode.

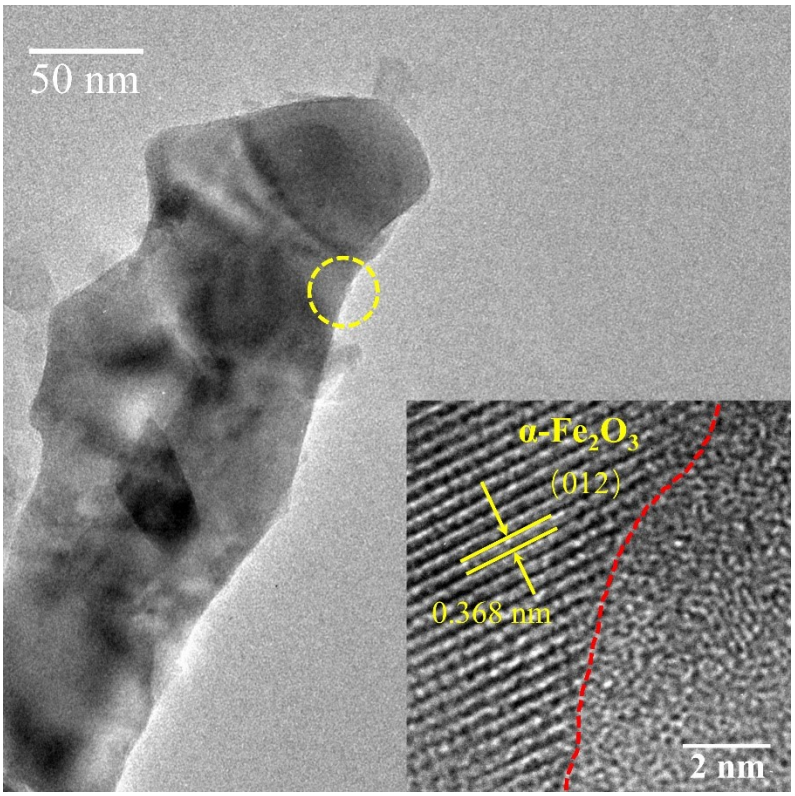

Fig. S7 TEM and HRTEM image of F photoanode.

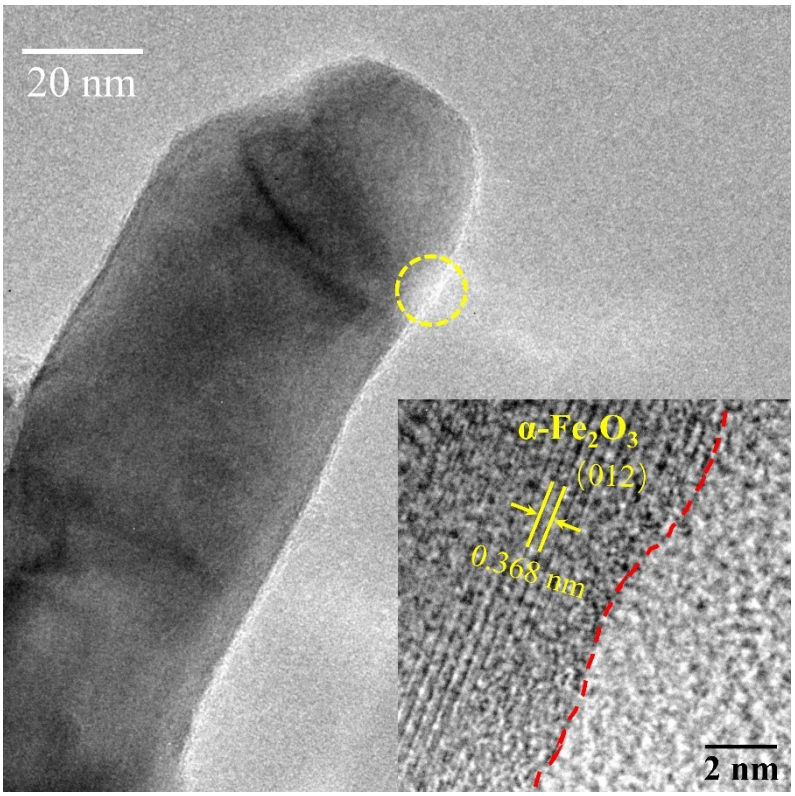

Fig. S8 TEM and HRTEM image of S-T-F photoanode.

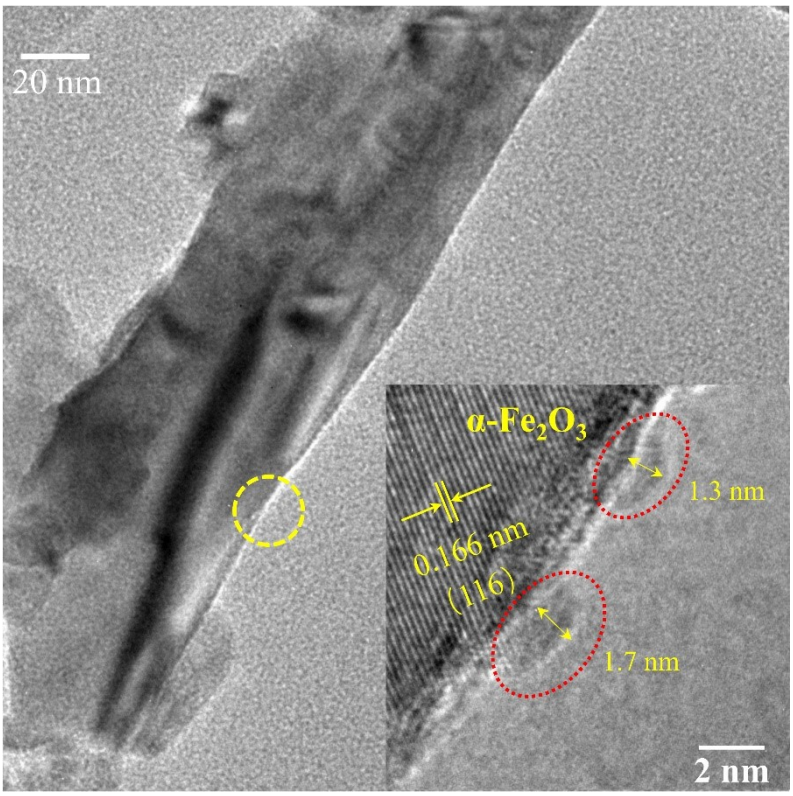

Fig. S9 TEM and HRTEM image of S-T-F/Z-1h.

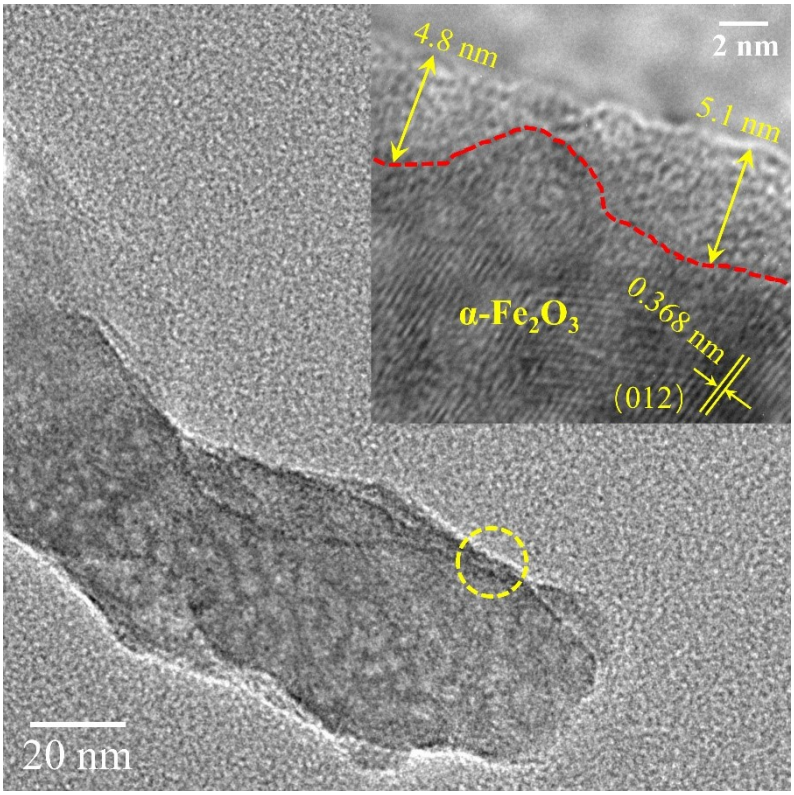

Fig. S10 TEM and HRTEM image of S-T-F/Z-3h.

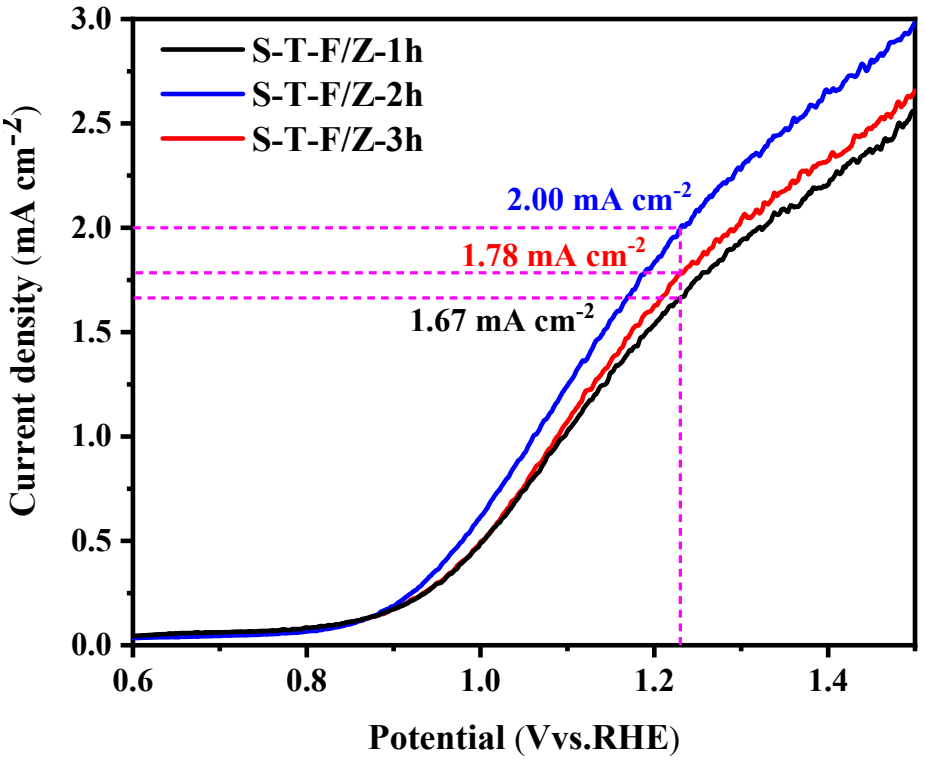

Fig. S11 Photocurrent density of S-T-F/Z after different solvothermal reaction time.

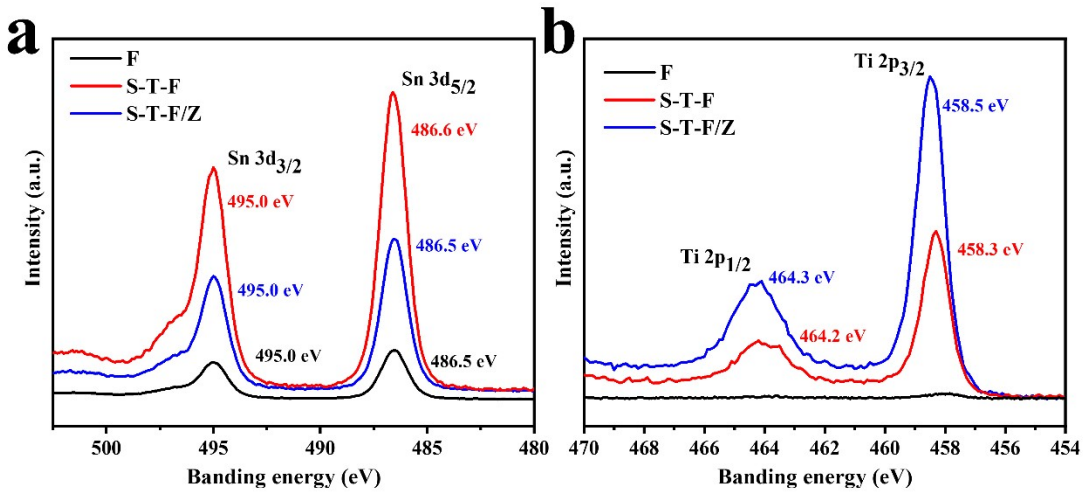

Fig. S12 (a) Sn 3d and (b) Ti 2p high-resolution XPS spectra of F, S-T-F and S-T-F/Z photoanode.

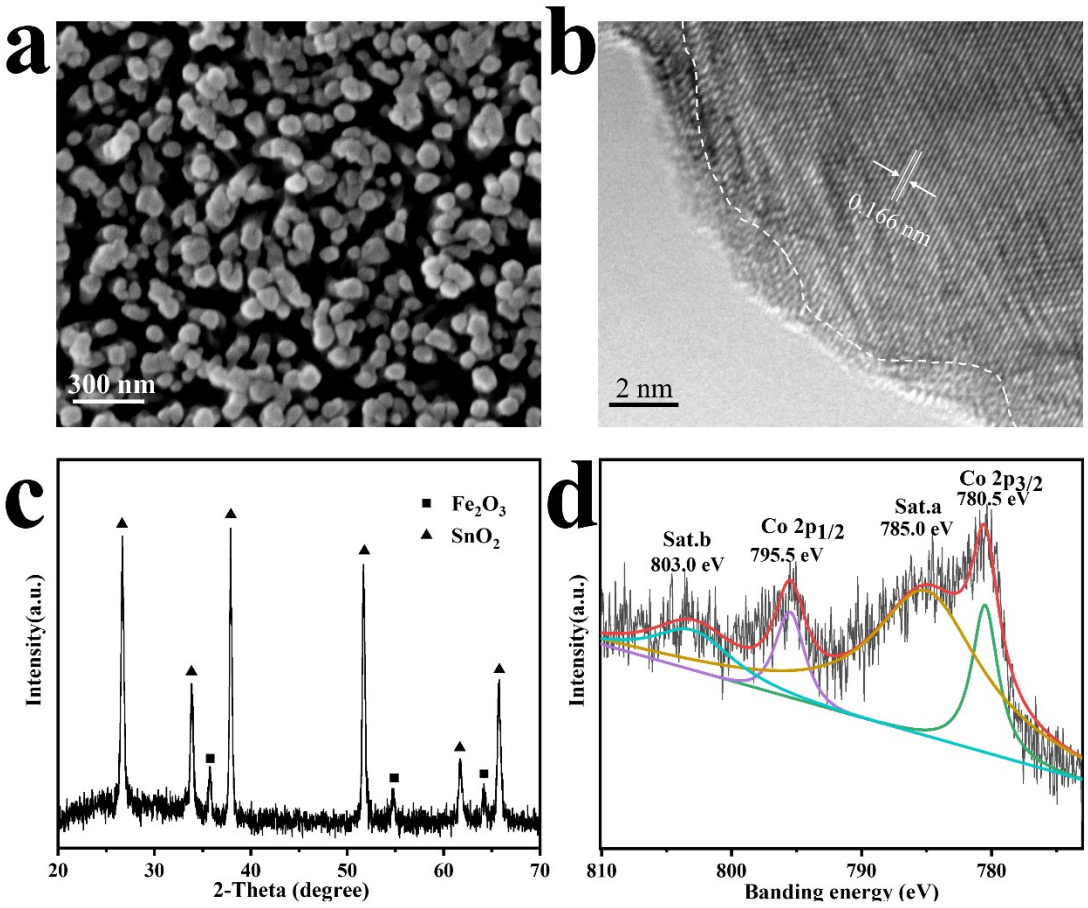

Fig. S13 (a) SEM, (b) TEM, (c) XRD patterns and (d) Co 2p XPS spectra of T-S-F/Z photoanode after the 10800s-photostability test, respectively.

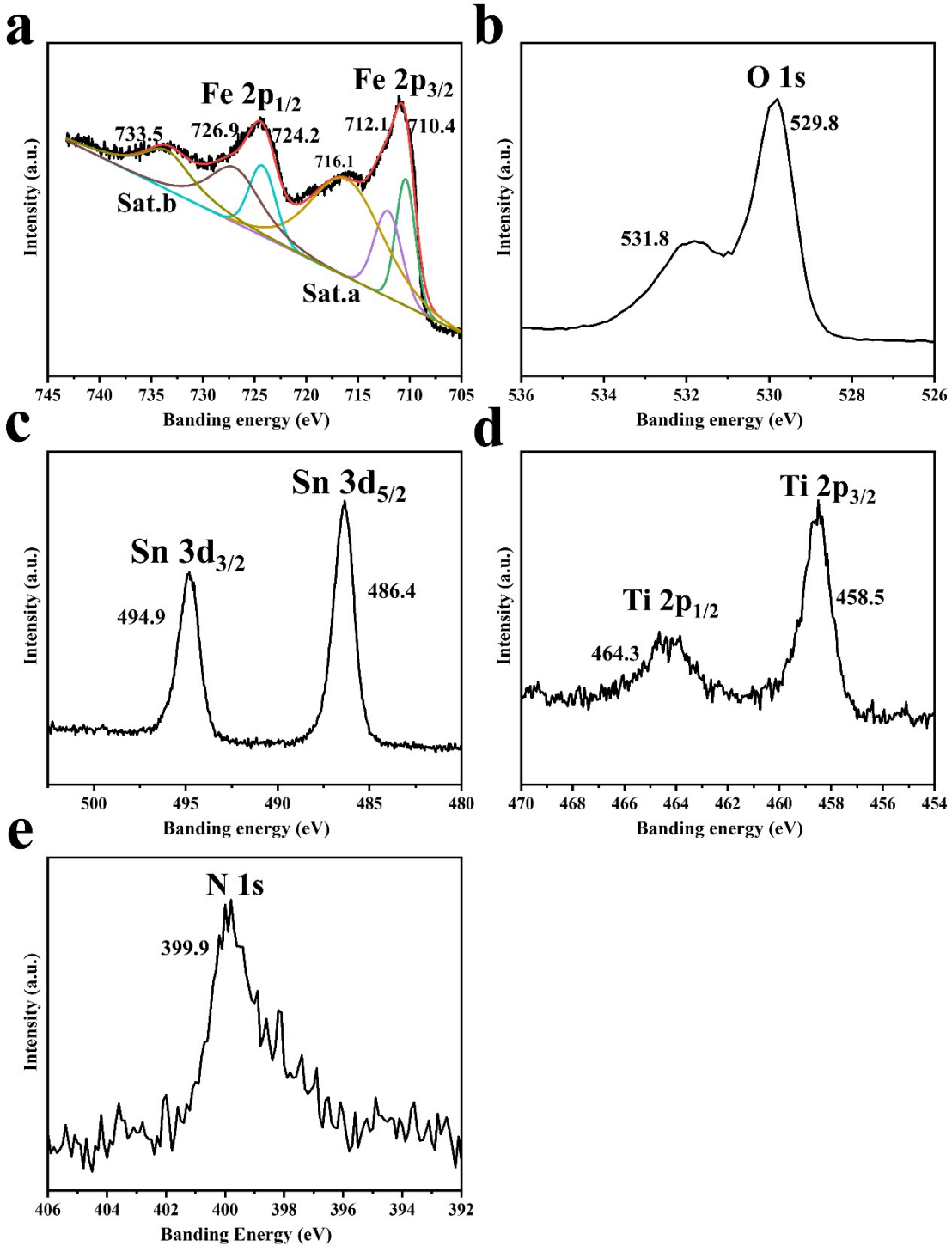

Fig. S14 (a) Fe 2p, (b) O 1s, (c) Sn 3d (d) Ti 2p and (e) N 1s spectra of S-T-F/Z photoanode after the 10800s-photostability test, respectively.

Table S1. TEM-EDX elemental analysis of S-T-F/Z including Fe, O, Ti, Sn, Co and N.

Element	Weight %	Atomic %
N	3.16	8.43
O	17.42	40.68
Ti	1.68	1.32
Fe	69.68	46.32
Co	2.29	1.45
Sn	5.77	1.79

Table S2. ICP-OES data including Fe, Sn, Ti and Co of different photoelectrodes.

Sample	Molar ratio of elements (%)*			
	Fe	Sn	Ti	Co
F (fresh)	99.24	0.76	0	0
S-T-F (fresh)	93.57	3.12	3.31	0
S-T-F/Z (fresh)	91.02	2.64	2.49	3.85
S-T-F/Z (used)	91.76	2.51	2.67	3.06

Table S3. Comparison of our Sn-Ti-Fe_2O_3/ZIF-67 photoanode to other α-Fe_2O_3-based photoanodes.

Photoanode	Photocurrent density at 1.23 V_{RHE} (mA cm^{-2})	Onset potential (V_{RHE})	IPCE (%) (at 1.23V_{RHE})	Ref.
Sn-Ti-Fe_2O_3/ZIF-67	2	0.9	38.3 (350 nm)	This work
CoO_x/$LaFeO_3$/Fe_2O_3	1.12	0.95	25.13 (400 nm)	[1]
CoPi/$CaFe_2O_4$/Fe_2O_3	1.06	0.88	23 (365 nm)	[2]
TiO_2/Fe_2O_3	1.79	0.88	no	[3]
CuO/Fe_2O_3	0.7	0.87	11.4 (365 nm)	[4]
MoS_2/W-Fe_2O_3	1.87	0.64	37 (325 nm)	[5]
Fe_2O_3@TiO_2	1.3	0.9	23 (350 nm)	[6]
MnO_2/P:Fe_2O_3	1.65	0.9	11.2 (350 nm)	[7]
S:Fe_2O_3	1.42	0.82	18.2 (350 nm)	[8]
FeOOH/Fe_2O_3	1.21	0.65	no	[9]
Mg-Fe_2O_3/Fe_2O_3 film	0.5	0.8	19 (300 nm)	[10]
nN^+ α-Fe_2O_3-TiO_2	1.1	1.06	no	[11]
FeOOH/Fe_2O_3@$FeTaO_4$	2.86	0.84	no	[12]
Fe_2O_3/Fe_3O_4	2	0.84	30 (340 nm)	[13]

References

1. Q. Peng, J. Wang, Z. J. Feng, C. Du, Y. W. Wen, B. Shan and R. Chen, *Journal of Physical Chemistry C*, 2017, **121**, 12991-12998.
2. M. G. Ahmed, T. A. Kandiel, A. Y. Ahmed, I. Kretschmer, F. Rashwan and D. Bahnemann, *Journal of Physical Chemistry C*, 2015, **119**, 5864-5871.
3. J. J. Deng, Q. Q. Zhuo and X. X. Lv, *Journal of Electroanalytical Chemistry*, 2019, **835**, 287-292.
4. J. Y. Ma, Q. Wang, L. L. Li, X. H. Zong, H. Sun, R. Tao and X. X. Fan, *Journal of Colloid and Interface Science*, 2021, **602**, 32-42.
5. Z. Masoumi, M. Tayebi, M. Kolaei, A. Tayyebi, H. Ryu, J. I. Jang and B. K. Lee, *Acs Applied Materials & Interfaces*, 2021, **13**, 39215-39229.
6. Y. G. Li, X. L. Wei, B. W. Zhu, H. Wang, Y. X. Tang, T. C. Sum and X. D. Chen, *Nanoscale*, 2016, **8**, 11284-11290.
7. Q. Rui, L. Wang, Y. J. Zhang, C. C. Feng, B. B. Zhang, S. R. Fu, H. L. Guo, H. Y. Hu and Y. P. Bi, *Journal of Materials Chemistry A*, 2018, **6**, 7021-7026.
8. R. Zhang, Y. Y. Fang, T. Chen, F. L. Qu, Z. Liu, G. Du, A. M. Asiri, T. Gao and X. P. Sun, *Acs Sustainable Chemistry & Engineering*, 2017, **5**, 7502-7506.
9. J. Y. Kim, D. H. Youn, K. Kang and J. S. Lee, *Angewandte Chemie-International Edition*, 2016, **55**,

10854-10858.

10. Y. J. Lin, Y. Xu, M. T. Mayer, Z. I. Simpson, G. McMahon, S. Zhou and D. W. Wang, *Journal of the American Chemical Society*, 2012, **134**, 5508-5511.
11. J. S. Yang, W. H. Lin, C. Y. Lin, B. S. Wang and J. J. Wu, *Acs Applied Materials & Interfaces*, 2015, **7**, 13314-13321.
12. H. Zhang, W. Y. Noh, F. Li, J. H. Kim, H. Y. Jeong and J. S. Lee, *Advanced Functional Materials*, 2019, **29**.
13. B. Lei, D. D. Xu, B. Wei, T. F. Xie, C. Y. Xiao, W. L. Jin and L. L. Xu, *Acs Applied Materials & Interfaces*, 2021, **13**, 4785-4795.